OCDM-Based Multi-Numerology Communications for 6G

Vincent Savaux

Date of publication xxxx 00, 0000, date of current version xxxx 00, 0000.

Digital Object Identifier 10.1109/ACCESS.2023.0322000

OCDM-Based Multi-Numerology Communications for 6G

VINCENT SAVAUX[1], (Senior Member, IEEE)
[1]Institute of Research and Technology b<>com, Rennes, France (e-mail: vincent.savaux@b-com.com)
Corresponding author: Vincent Savaux (e-mail: vincent.savaux@b-com.com).

ABSTRACT This paper deals with the capability of the orthogonal chirp division multiplexing (OCDM) modulation scheme to cope with multi-numerology concept in the context of next generations of communications. The OCDM-based multi-numerology transceiver is introduced, and the inter-numerology interference (INI) is analytically derived. The case of filtered-OCDM is considered as well, allowing to both reduce the INI and to shape the power spectrum of the composite signal (*i.e.* the signal composed of unitary signals configured with different numerologies) according to strong constraints of low out-of-band emissions. The simulations results show the inherent robustness of OCDM against INI as the interference is spread over all subcarriers, whereas it is concentrated in particular subcarriers in OFDM. It results that the (filtered)-OCDM waveform largely outperforms the orthogonal frequency division multiplexing (OFDM) by more than 2 dB in term of bit error rate (BER) performance, without need for a guard-band between numerologies.

INDEX TERMS OCDM, Multi-numerology, 6G, OFDM.

IEEE Access
Multidisciplinary | Rapid Review | Open Access Journal

Date of publication xxxx 00, 0000, date of current version xxxx 00, 0000.

Digital Object Identifier 10.1109/ACCESS.2023.0322000

OCDM-Based Multi-Numerology Communications for 6G

VINCENT SAVAUX[1], (Senior Member, IEEE)
[1]Institute of Research and Technology b<>com, Rennes, France (e-mail: vincent.savaux@b-com.com)
Corresponding author: Vincent Savaux (e-mail: vincent.savaux@b-com.com).

I. Introduction

Multi-numerology has been introduced in 5G new radio (NR) to offer flexibility in the choice of the orthogonal frequency division multiplexing (OFDM) waveform parameters in order to cope with the multiples applications and services (*e.g.* low latency or broadband communications), and to adapt the signal to the propagation environment [1], [2]. The main parameters that can be configured, among others, are the subcarrier spacing (or equivalently the symbol duration) and the cyclic prefix length. In particular, the subcarrier spacing can be chosen among $\{15.2^{\mu}|\mu = 0, 1, .., 6\}$ kHz such as defined in the standard [3]. Furthermore, the 5G NR allows for the transmission of composite signals consisting of multiple unitary signals sharing contiguous sub-bands within a common band, each of them being configured with a specific numerology. However, despite the gain of flexibility, such multi-numerology signals suffer from inter-numerology interference (INI) due to the loss of orthogonality between neighboring signals that do not share the same numerology.

The INI in OFDM-based multi-numerology systems has been deeply analyzed in [4]–[6] and some solutions aiming at mitigating or cancelling INI have been proposed in the literature. The most common technique consists in inserting a guard-band between sub-bands [7], to the cost of a loss of spectral efficiency. To better improve the spectral efficiency, it is suggested in [8] to insert data subcarriers within the guard-band, the indices of which are chosen according to a limited increase of INI. In [4], the authors consider the windowed-OFDM scheme to mitigate the INI, and an iterative algorithm at the receiver side to cancel most of the remaining interference. Otherwise, the cancellation is carried out at the transmitter side in [9], where a pre-equalization stage can be applied since the transmitted data is known. In [5], [6], the INI is reduced by using a common CP shared by several OFDM symbols instead of the conventional per-symbol CP insertion [3], in order to better align the OFDM symbols among different numerologies. Alternatively, the authors of [10] base their methods for INI reduction on the scheduling of the different users sharing the sub-bands: power scheduling or scheduling managed by machine learning algorithm. However, all these methods are based on OFDM systems, and only few papers mention other waveforms such filter-bank multicarrier (FBMC) as solutions for multi-numerology communications [2], but this waveform has not been held as a solution in 5G NR.

More recently, new waveforms have been suggested as interesting alternatives to OFDM and are serious candidates for 6G communications [11], such as orthogonal time frequency space (OTFS) modulation [12], orthogonal chirp division multiplexing (OCDM) [13], and affine function division multiplexing (AFDM) [14]–[16]. The advantages of these modulation schemes lie in their inherent optimality (in term of decoding capability) against time and frequency selective channels [17], [18] whereas OFDM is only sub-optimal against frequency selective channels, and they are also relevant in the context of sensing and communications in 6G [11]. These good properties are due to the fact that these modulations spread the errors from the environment (multipath, Doppler, interference) over the time and frequency grid. In addition, OCDM has proven to be backward compatible with OFDM [19], [20], since it can be seen as a chirp-precoded OFDM involving simple (I)DFT-based (de)modulation. This latter property offers the additional advantage to OCDM to be easily implemented and deployed in existing and future communications systems, whereas other modulation schemes such as FBMC, OTFS, and AFDM require dedicated (de)modulation processes which still limit their implementation.

In this paper, we suggest to apply the OCDM waveform in the context of multi-numerology, based on the aforementioned reasons of robustness against errors and backward compatibility with OFDM. To this end, we first present in detail the OCDM-based multi-numerology transceiver built from the generic DFT-based OCDM modulation in [19], [20], and the resulting signals in both frequency and time domains.

This is then extended to the case of filtered-OCDM using the same filter as in [19], [21], which allows for a drastic reduction of both INI and out-of-band emission, making the composite signal compliant with spectrum scarcity use cases. From this system model, we provide a theoretical analysis of the INI from which we observe that the interference should actually be spread over all subcarrier thanks to the chirps, unlike OFDM where INI is concentrated on the edge subcarriers. This result is confirmed through simulations and we show that (filtered-)OCDM largely outperforms (filtered-)OFDM in terms of bit error rate (BER) performance without need of guard-band, demonstrating the relevance of (filtered-)OCDM in the context of multi-numerology systems. Thus, the contributions of this paper are summarized as follows:

- We introduce the OCDM-based multi-numerology system model, and we extend to the filtered-OCDM multi-numerology, based on the DFT-precoded OCDM model,
- We analyze the INI inherent to the system, and we show that the INI is spread over the whole subcarriers thanks to the OCDM modulation scheme,
- We highlight through simulations that the OCDM outperforms the OFDM in the context of multi-numerology.

The rest of this paper is organized as follows: Section II presents the OCDM waveform, and Section III introduces how it is applied in multi-numerology system. In Section IV, the signal at receiver side is described, from which the INI are analytically expressed. Section V is dedicated to simulations results, and Section VI concludes this paper.

II. OCDM System Model

This section presents the OCDM waveform, and how it can be described as precoded OFDM, where the precoding step consists in a DFT and a multiplication by a chirp. The OCDM modulation scheme is an emerging waveform which is based on Fresnel transform instead of Fourier transform as in OFDM. Thus, the samples x_n of the OCDM signal x, when it is sampled at Nyquist rate, is defined as the inverse discrete Fresnel transform of the symbols of constellation $\{C_0, C_1, .., C_{N-1}\}$ [13], where $n = 0, 1, .., N-1$ is the time sample index and N is the number of subcarriers (in OCDM the subcarriers refers to chirps instead of sinusoids as in OFDM):

$$x_n = \frac{e^{j\frac{\pi}{4}}}{N} \sum_{k=0}^{N-1} C_k \times \begin{cases} e^{-j\frac{\pi}{N}(n-k)^2}, & \text{if } N \text{ even} \\ e^{-j\frac{\pi}{N}(n-k+\frac{1}{2})^2}, & \text{if } N \text{ odd} \end{cases}. \quad (1)$$

It has been shown in [19], [20] that the OCDM signal x is similar to a pre-coded OFDM signal where the precoding step consists in a DFT of $\{C_0, C_1, .., C_{N-1}\}$, followed by the multiplication by the chirp $e^{j\frac{\pi m^2}{N}}$, where $m = 0, 1, .., N-1$ is the frequency domain index. This is illustrated in Fig. 1, where one of the two branches should be considered for single-numerology OCDM modulation (Fig. 1 is more general as it considers multi-numerology). Thus, the samples X_m in the frequency domain, *i.e.* after precoding and previous to IDFT step, are given in Proposition 1.

Proposition 1. *For any $m = 0, 1, .., N-1$, the samples $X_m = DFT(x_n)$ are expressed as*

$$X_m = \frac{\sqrt{N}}{N^2} \sum_{k=0}^{N-1} C_k \times \begin{cases} e^{j\frac{\pi}{N}(m^2-2km)}, & \text{if } N \text{ even} \\ e^{j\frac{\pi}{N}(m^2+m(1-2k))}, & \text{if } N \text{ odd} \end{cases}. \quad (2)$$

Proof: See Appendix A.

It results from (2) that the time samples x_n of the OCDM signal in (1) can be rewritten as

$$x_n = \sum_{m=0}^{N-1} X_m e^{2j\pi\frac{mn}{N}}. \quad (3)$$

More general formulations of the OCDM modulation have been suggested in [19], [20], to consider an OCDM signal sampled at a frequency higher than Nyquist rate. In that case, we introduce $K \leq N$ as the number of useful subcarriers, and Q the number of null subcarriers that are mapped at the edges of the spectrum. Thus, we assume that $N = K + 2Q$ holds, where N is the IDFT size, and the same number Q null subcarriers are considered at both edges of the spectrum. In that case, the samples of the OCDM signal can be expressed as

$$x_n = \sum_{m=0}^{N-1} \alpha_m \underbrace{\frac{\sqrt{K}}{KN} e^{j\pi\frac{(m-Q)^2}{K}} \left[\sum_{k=0}^{K-1} C_k e^{-2j\pi\frac{k(m-Q)}{K}} \right]}_{X_m} e^{2j\pi\frac{mn}{N}}, \quad (4)$$

with $\alpha_m = 0$ if the m-th subcarrier is null, and $\alpha_m = 1$ otherwise. In the following, we introduce a more general model fitting the multi-numerology constraints. Moreover, we limit to the case where N (resp. K) is even in order to ease the notations, but all the developments remain valid in the case where N (resp. K) is odd.

III. OCDM-Based Multi-numerology Signal

We consider a multi-numerology system composed of two signals x^{NS} and x^{WS} sharing the same frequency resource of bandwidth B_w. The superscripts *NS* and *WS* refer to narrow and wide subcarrier spacing, respectively. The corresponding subcarrier spacing is defined as $\Delta_f^{NS} = \frac{B_w}{N}$ and $\Delta_f^{WS} = \frac{B_w}{M}$, where N and M are the subcarriers numbers of the NS and WS systems, respectively. Furthermore, according to the 5G standard, we assume that the ratio $R = \frac{N}{M}$ is a power of 2, allowing for a time alignment of the signals. Fig. 1 shows the block-diagram of the OCDM-based multi-numerology transmitter, including the precoding step per branch such as previously detailed, the addition of null subcarriers, the IDFT, the cyclic prefix (CP) addition, and a possible filtering step (referred to "Fil." within the dashed box). Then the multi-numerology composite signal is created by the addition of 1 symbol x^{NS} and R symbols x^{WS}. The signals can be isolated in frequency by the addition of a frequency guard band Δ_f, which is assumed to be a multiple of Δ_f^{NS}. Note that we limit

to a model involving two numerologies, but such as emphasized in [6], the case where more than two numerologies are transmitted can be straightforwardly tackled by considering one pair of numerologies at a time. A detailed description of the signals x^{NS} and x^{WS} in both the frequency and time domains, as well as the composite signal, is hereby provided.

A. FREQUENCY DOMAIN

According to the OCDM signal described in (2), the frequency samples X_m^{NS} of the NS signal are given by (5), where K_N is the number of data subcarriers, Q_N is the number of null subcarriers at the edge of the band (we arbitrarily define it as the bottom edge of the band). The remaining $P_N = N - Q_N + K_N$ zero subcarriers with indices $Q_N + K_N \leq m \leq N-1$ gather the possible frequency guard band, the subcarriers dedicated to the WS signal, and the null subcarriers at the upper edge of the band. The frequency samples $X_{m'}^{WS}$ of the WS signal can in turn be expressed as in (6), where K_W is the number of data subcarriers, and Q_W gather the possible frequency guard band, the subcarriers dedicated to NS signal, and the null subcarriers at the bottom edge of the band. The remaining value $P_W = M - (Q_W + K_W)$ corresponds to the zero subcarriers at the upper edge of the band. Fig. 2 illustrates the partition of the band in a time-frequency view of the system model.

To further detail the relationship between the values defined in both numerologies, it must be emphasized that the following equalities hold:

$$\begin{aligned} P_N = N - (Q_N + K_N) &= \frac{\Delta_f}{\Delta_f^{NS}} + R(M - Q_W) \\ Q_W &= \frac{1}{R}\left(\frac{\Delta_f}{\Delta_f^{NS}} + Q_N + K_N\right), \end{aligned} \tag{7}$$

where $\frac{\Delta_f}{\Delta_f^{NS}}$ is equal to the number of NS subcarriers in the the guard band. It must be noticed that, by construction, $\frac{\Delta_f}{\Delta_f^{NS}} + Q_N + K_N$ is a multiple of R.

B. TIME DOMAIN

According to (3) and (4), the time-domain samples of the NS and WS signals after IFFT blocks are given by:

$$x_n^{NS} = \sum_{m=0}^{N-1} X_m^{NS} e^{2j\pi \frac{mn}{N}}, \tag{8}$$

where $0 \leq n \leq N-1$, and

$$x_{n'}^{WS} = \sum_{m'=0}^{M-1} X_{m'}^{WS} e^{2j\pi \frac{m'n'}{M}}. \tag{9}$$

where $0 \leq n' \leq M-1$. We define N_{CP} the size of the CP for the NS signal. After the CP addition, the sample index n varies within $0 \leq n \leq N + N_{CP} - 1$, and then x_n^{NS} becomes:

$$x_n^{NS,CP} = \sum_{m=0}^{N-1} X_m^{NS} e^{2j\pi \frac{m}{N}((n-N_{CP}) \mod N)}. \tag{10}$$

Similarly to the case NS, we define M_{CP} the size of the CP for the WS signal, such that we have $\frac{N_{CP}}{M_{CP}} = R$. Then, for any $r = 0, 1, .., R-1$, the samples $x_{n',r}^{WS,CP}$ of the r-th symbol among the R concatenated WS OCDM symbols, can be expressed as

$$x_{n',r}^{WS,CP} = \sum_{m'=0}^{M-1} X_{m',r}^{WS} e^{2j\pi \frac{m'}{M}((n'-M_{CP}) \mod M)}, \tag{11}$$

where $0 \leq n' \leq M + M_{CP} - 1$. Note that $x^{NS,CP}$ and $x_r^{WS,CP}$ are sampled at the same rate but $x^{NS,CP}$ is R times longer than $x_r^{WS,CP}$ (in number of samples). In order for $x^{NS,CP}$ and $x_r^{WS,CP}$ to share the same sample index basis, we set $n = n' + r(M + M_{CP})$, then the samples $x_{n,r}^{WS,CP}$ can be rewritten as in (12).

Finally, the composite signal samples, denoted by x_n^{CP}, $n = 0, 1, .., N + N_{CP} - 1$, consists in the sum of $x_n^{NS,CP}$ in (10) and the R symbols $x_{n,r}^{WS,CP}$ (12), which yields:

$$x_n^{CP} = x_n^{NS,CP} + \underbrace{\gamma \sum_{r=0}^{R-1} x_{n,r}^{WS,CP}}_{x_n^{WS,CP}}, \tag{13}$$

where we define $x^{WS,CP}$ as the signal gathering the R concatenated symbols $x_r^{WS,CP}$, and γ is a real coefficient that allows to possibly adjust the power of $x^{WS,CP}$ compared to that of $x^{NS,CP}$. It is worth noticing that the generation of the composite signal in (13) is an irreversible operation, in the sense that it is impossible at the receiver side to perfectly recover the samples $x_n^{NS,CP}$ (resp. $x_{n,r}^{WS,CP}$) without interference from $x_{n,r}^{WS,CP}$ (resp. $x_n^{NS,CP}$). The main reason leading to this loss of orthogonality is the difference between the lengths of the reception windows: N for the signal x^{NS} therefore catching the R symbols $x_r^{WS,CP}$ (including the CPs), M for x_r^{WS} therefore only partially catching samples of $x^{NS,CP}$. Such as aforementioned, the solution called common CP proposed in [5], [6] for OFDM multi-numerology system allows to reduce the INI, but we do not focus on it in this paper (however note that it could be straightforwardly adapted from OFDM to OCDM). We rather take advantage of the inherent robustness of OCDM against interference to show the relevance of OCDM to be used in multi-numerology communications systems. Furthermore, we also investigate the effect of a filtering stage (highlighted by the block "Fil." in Fig. 1), which constrains the shape of the signal spectrum therefore limiting the out-of-band emission, and in turn the INI. The design of the considered filters is hereby described, in order to fit the features of the NS and WS components of the composite signal.

C. FILTERED OCDM

The principle of filtered OCDM is to add a given filter at both transmitter and receiver sides to better shape the spectrum with respect to low out-of-band emission constraints. In this paper, we consider a very similar filter as in [19], [21], as it is compliant with 3GPP proposition [21]. However, we cannot directly apply the low-pass filter as in [19], since none of

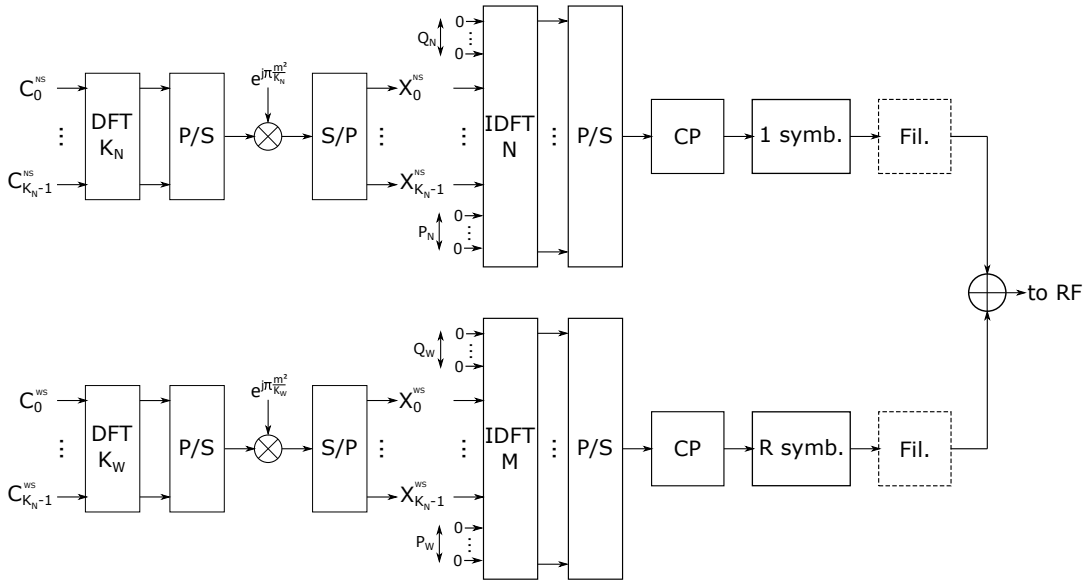

FIGURE 1. **OCDM-based multi-numerology at transmitter: the top (resp. bottom) branch corresponds to the NS (resp. WS).**

$$X_m^{NS} = \begin{cases} 0, & 0 \le m \le Q_N - 1 \\ \frac{e^{j\pi \frac{(m-Q_N)^2}{K_N}}}{\sqrt{K_N N}} \sum_{k=0}^{K_N-1} C_k^{NS} e^{-2j\pi \frac{k(m-Q_N)}{K_N}}, & Q_N \le m \le Q_N + K_N - 1 \\ 0, & Q_N + K_N \le m \le N-1 \end{cases}, \tag{5}$$

$$X_{m'}^{WS} = \begin{cases} 0, & 0 \le m' \le Q_W - 1 \\ \frac{e^{j\pi \frac{(m'-Q_W)^2}{K_W}}}{\sqrt{K_W M}} \sum_{k=0}^{K_W-1} C_k^{WS} e^{-2j\pi \frac{k(m'-Q_W)}{K_W}}, & Q_W \le m' \le Q_W + K_W - 1 \\ 0, & Q_W + K_W \le m' \le M-1 \end{cases}, \tag{6}$$

$$x_{n,r}^{WS,CP} = \begin{cases} \sum_{m'=0}^{M-1} X_{m',r}^{WS} e^{2j\pi \frac{m'}{M}((n-M_{CP}-r(M+M_{CP})) \mod M)}, & \text{if } r(M+M_{CP}) \le n \le (r+1)(M+M_{CP})-1 \\ 0, \text{ else} \end{cases}. \tag{12}$$

the NS and WS components of the multi-numerology OCDM signal is strictly baseband, *i.e.* centered according to the null frequency. Thus, two band-pass filters denoted g^{NS} and g^{WS} must be created to match the frequency offsets inherent to x^{NS} and x^{WS}. Thus, according to [19], [21], the two filters can be generally defined as

$$g_n^i = \frac{p_n^i w_n^i}{\sum_n p_n^i w_n^i} e^{2j\pi \frac{\theta^i}{N^i} n}, \tag{14}$$

where the superscript i refers to NS or WS, θ^i and N^i are the corresponding frequency offset and length of the signal, and $-\lfloor \frac{L_f^i}{2} \rfloor \le n \le \lfloor \frac{L_f^i}{2} \rfloor$, with L_f^i the length of the filter. It must be noted that, according to Fig. 1, we apply the filter g_n^{WS} to the whole signal $x^{WS,CP}$ (*i.e.* not to each of the R symbols $x_r^{WS,CP}$). As a consequence, $N^i = N$ holds for any i, and then the frequency offsets are given by:

$$\theta^{NS} = Q_N + \frac{K_N}{2} - \frac{N}{2}, \tag{15}$$

and

$$\theta^{WS} = R(Q_W + \frac{K_W}{2}) - \frac{N}{2}, \tag{16}$$

where the term $\frac{N}{2}$ in (15) and (16) highlights the fact that the null frequency (DC carrier) corresponds to the center of the band, namely the $(\frac{N}{2}+1)$-th subcarrier. The general filter g^i in (14) is composed of a *sinc* function p^i and a generalized low-pass filter w^i. The samples p_n^i are given by:

$$p_n^i = \text{sinc}\left(\frac{K^i + 2\delta_w^i}{N}.n\right), \tag{17}$$

where $K^{NS} = K_N$ (reps. $K^{WS} = R.K_W$) in the case of the NS signal (resp. WS signal), and δ_w^i is the so-called tone offset,

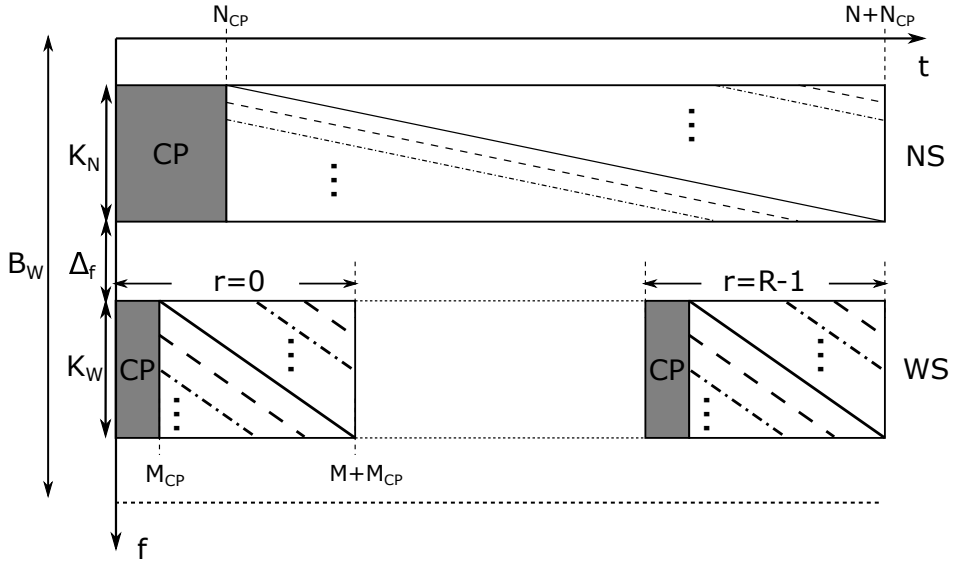

FIGURE 2. Time-frequency representation of OCDM-based multi-numerology.

which ensures that the resulting filter has a flat passband over the entire signal bandwidth. The samples w_n^i are given by:

$$w_n^i = \left(0.5\left(1+\cos\left(\frac{2\pi n}{L_f^i - 1}\right)\right)\right)^{0.6}. \tag{18}$$

Different examples of filter shape are provided in [21] according the length of the filter and the DFT size. As a rule of thumb, the longer the filter, the lower the out-of-band emission, to the cost of an increase of the complexity. Finally, the composite signal composed of two filtered signals, denoted by $x^{CP,f}$, can be expressed as

$$x^{CP,f} = (g^{NS} * x^{NS,CP}) + (g^{WS} * x^{WS,CP}), \tag{19}$$

where $(. * .)$ is the convolution. Note that (19) is a general expression, but filtering can be applied to both signals or only one. The effect of the filter will be numerically shown in Section V.

IV. Inter-Numerology Interference

This section aims at describing the receiver adapted to the multi-numerology OCDM communication scheme, as well as to evaluate the per-subcarrier INI.

A. OCDM-BASED MULTI-NUMEROLOGY RECEIVER

Similarly to the transmitter, the OCDM-based multi-numerology receiver consists in a two-branch (or more than 2 branches) processing including, in each branch, the CP removal, the DFT (of size M for WS or N for NS), the null subcarrier removal, the multiplication by the conjugate chirp $e^{-j\pi\frac{m}{K_i}}$, where $m = 0, 1, .., K_i - 1$ and $K_i = K_N$ or $K_i = K_W$, and a IDFT of size K_i. Fig. 3 illustrates one branch (NS or WS) of the OCDM-based multi-numerology receiver. Note that these processes are applied to the R symbols in case of WS. Possibly, the filter described in (14) is added previously to the CP removal.

We denote by y^{NS} and y^{WS} the received signals after CP removal in NS and WS reception branches, respectively. Ignoring the additive Gaussian noise, the samples y_n^{NS}, with $0 \le n \le N-1$, can be expressed as

$$\begin{aligned} y_n^{NS} &= x_n^{NS} + y_n^{WS,I} \\ &= x_n^{NS} + \sum_{r=0}^{R-1} y_{n,r}^{WS,I}, \end{aligned} \tag{20}$$

where $y_n^{WS,I}$ is the interfering signal from WS to NS, and the samples $y_{n,r}^{WS,I}$ are defined as in (21).

Similarly, the samples y_n^{WS} can be expressed as

$$y_n^{WS} = \sum_{r=0}^{R-1} x_{n,r}^{WS} + y_{n,r}^{NS,I}, \tag{22}$$

where $x_{n,r}^{WS}$ are the samples of the r-th WS symbol after CP removal, given by

$$x_{n,r}^{WS} = \begin{cases} \sum_{m'=0}^{M-1} X_{m',r}^{WS} e^{2j\pi\frac{m'}{M}(n-rM)}, \\ \text{if } rM \le n \le (r+1)M-1 \\ 0, \\ \text{else} \end{cases}, \tag{23}$$

and $y_{n,r}^{NS,I}$ are the samples of the interfering signal from NS to the r-th symbol of WS. We can reasonably suppose that the size of the WS symbols is larger than the length of the NS CP, namely $M + M_{CP} \ge N_{CP}$, then $y_{n,r}^{NS,I}$ yields

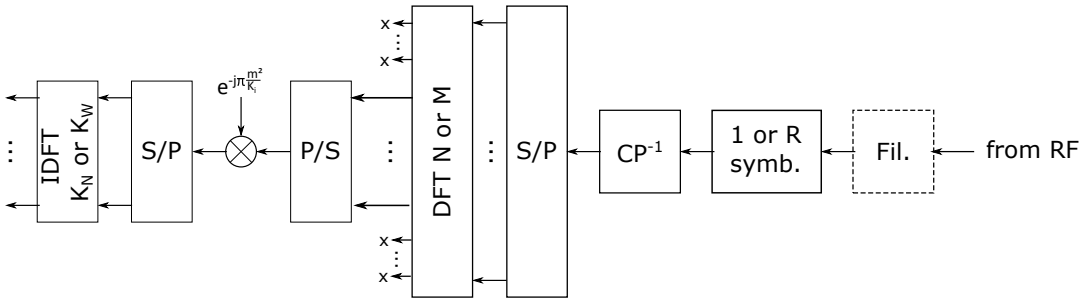

FIGURE 3. One branch of the OCDM-based multi-numerology receiver.

$$y_{n,r}^{WS,I} = \begin{cases} \sum_{m'=0}^{M-1} X_{m',0}^{WS} e^{2j\pi \frac{m'}{M}(n+N_{CP}-M_{CP})}, \text{ if } 0 \leq n \leq M+M_{CP}-N_{CP}-1 \text{ and } r=0 \\ \sum_{m'=0}^{M-1} X_{m',r}^{WS} e^{2j\pi \frac{m'}{M}((n+N_{CP}-M_{CP}-r(M+M_{CP})) \mod M)}, \\ \text{if } r(M+M_{CP})-N_{CP} \leq n \leq (r+1)(M+M_{CP})-N_{CP}-1 \text{ and } r>0 \\ 0, \text{ else} \end{cases}. \quad (21)$$

$$y_{n,r}^{NS,I} = \begin{cases} \sum_{m=0}^{N-1} X_m^{NS} e^{2j\pi \frac{m}{N}((n+M_{CP}-N_{CP}) \mod N)}, \\ \text{if } 0 \leq n \leq M-1 \text{ and } r=0 \\ \sum_{m=0}^{N-1} X_m^{NS} e^{2j\pi \frac{m}{N}(n+(r+1)M_{CP}-N_{CP})}, \\ \text{if } rM \leq n \leq (r+1)M-1 \text{ and } r>0 \\ 0, \text{ else} \end{cases}. \quad (24)$$

B. PER SUBCARRIER INI

1) From WS to NS

Similarly to the work carried out in [6] for OFDM-based multi-numerology waveform, we can assess the per subcarrier INI from WS to NS in OCDM, denoted $\chi_{k'}^{WS}$ for any $k' = 0, 1, .., K_N - 1$. It can be generally expressed from $y_n^{WS,I}$ in (20) as in (25), where A highlights the DFT of size N, and B the multiplication by the conjugate chirp and the IDFT of size K_N. The indices p' refers to the frequency index (at the output of the DFT).

After some developments that are provided in Appendix B, $\chi_{k'}^{WS}$ can be rewritten as:

$$\chi_{k'}^{WS} = \sum_{r=0}^{R-1} \chi_{k',r}^{WS}, \quad (26)$$

where

$$\chi_{k',r}^{WS} = \frac{e^{-2j\pi Q_N \Gamma_r}}{N} \sum_{p'=0}^{K_N-1} \sum_{m=0}^{M-1} X_{m,r}^{WS} e^{2j\pi \frac{m}{M}(N_{CP}-M_{CP})} \times \text{asinc}_{D_r}\left(\frac{m}{M} - \frac{p'+Q_N}{N}\right) e^{-j\pi \frac{p'^2}{K_N}} e^{2j\pi \frac{k'p'}{K_N}} e^{-2j\pi p' \Gamma_r}, \quad (27)$$

where asinc_{D_r} is the so-called aliased *sinc* function defined for any $x \in \mathbb{R}$ as

$$\text{asinc}_{D_r}(x) = \frac{1-e^{2j\pi D_r x}}{1-e^{2j\pi x}}, \quad (28)$$

with

$$D_r = \begin{cases} M+M_{CP}-N_{CP}, & \text{if } r=0 \\ M+M_{CP}, & \text{if } 1 \leq r \leq R-1 \end{cases}, \quad (29)$$

and

$$\Gamma_r = \begin{cases} 0, & \text{if } r=0 \\ r(M+M_{CP})-N_{CP}, & \text{if } 1 \leq r \leq R-1 \end{cases}. \quad (30)$$

Although it seems difficult to interpret (26) and (27) directly, an analysis will be provided hereafter.

2) From NS to WS

We denote by $\chi_{k',r}^{NS}$ the per subcarrier INI from NS to the r-th WS symbol for any $k' = 0, 1, .., K_N - 1$ and $r = 0, 1, .., R-1$. From the expression of $y_{n,r}^{NS,I}$ in (24), and according to the developments carried out in Appendix C, $\chi_{k',r}^{NS}$ can be expressed as in (31), where we define $\psi_{p',r}^{WS}$ for the purpose of further analysis.

Such as previously mentioned for (26)-(27), it may be difficult to directly analyze (31). However, it can be noticed that, for K_N sufficiently large (at least $K_N > 10$, which is a reasonable assumption), and assuming that the symbols of constellation C_k are independent and identically distributed with $\mathbb{E}\{C_k^{NS}\} = 0$, then by the central limit theorem we obtain that X_m^{NS} are zero-mean complex Gaussian variables with variance denoted by σ_x^2. By supposing for clarity purpose that the constellation is normalized, *i.e.* $\mathbb{E}\{|C_k^{NS}|^2\} = 1$, σ_x^2 can be expressed from (5) and for any $Q_N \leq m \leq Q_N + K_N - 1$ as

$$\chi_{k'}^{WS} = \underbrace{\sum_{p=Q_N}^{Q_N+K_N-1} \overbrace{\left[\frac{1}{N}\sum_{n=0}^{N-1} y_n^{WS,I} e^{-2j\pi\frac{pn}{N}}\right]}^{A} e^{-j\pi\frac{(p-Q_N)^2}{K_N}} e^{2j\pi\frac{k'(p-Q_N)}{K_N}}}_{B}, \tag{25}$$

$$\chi_{k',r}^{NS} = \frac{1}{M}\sum_{p'=0}^{K_W-1} \underbrace{\sum_{m=0}^{N-1} X_m^{NS} e^{2j\pi\frac{m}{N}((r+1)M_{CP}-N_{CP})} \text{asinc}_M\left(\frac{m}{N} - \frac{p'+Q_W}{M}\right)}_{\psi_{p',r}^{WS}} e^{-j\pi\frac{p'^2}{K_W}} e^{2j\pi\frac{k'p'}{K_W}}, \tag{31}$$

$$\begin{aligned}\sigma_x^2 =& \mathbb{E}\{|X_m^{NS}|^2\} \\ =& \frac{1}{K_N N^2}\sum_{k=0}^{K_N-1} \mathbb{E}\{|C_k^{NS}|^2 \\ =& \frac{1}{N^2}.\end{aligned} \tag{32}$$

Thus, the samples X_m^{NS} can be interpreted as WGN. Besides, under the assumption of independence of the samples, then $\psi_{p',r}^{WS}$ can in turn be considered as a complex Gaussian variable with mean $\mu_{p'}$ and variance $\sigma_{p'}^2$. Since X_m^{NS} are zero-mean, it is trivial that

$$\mu_{p'} = \mathbb{E}\{\psi_{p',r}^{WS}\} = 0. \tag{33}$$

Furthermore, by applying Euler's identity, we find that $\sigma_{p'}^2$ is given by:

$$\begin{aligned}\sigma_{p'}^2 =& \mathbb{E}\{|\psi_{p',r}^{WS}|^2\} \\ =& \sum_{m=Q_N}^{Q_N+K_N-1} \mathbb{E}\{|X_m^{NS}|^2\} \frac{\sin(\pi M(\frac{m}{N} - \frac{p'+Q_W}{M}))^2}{\sin(\pi(\frac{m}{N} - \frac{p'+Q_W}{M}))^2} \\ =& \frac{1}{N^2}\sum_{m=Q_N}^{Q_N+K_N-1} \frac{\sin(\pi M(\frac{m}{N} - \frac{p'+Q_W}{M}))^2}{\sin(\pi(\frac{m}{N} - \frac{p'+Q_W}{M}))^2}.\end{aligned} \tag{34}$$

It must be emphasized that this result matches those obtained in [6] for OFDM systems. Thus, $\psi_{p',r}^{WS}$ can be considered as a colored noise. Then, applying an IDFT to this colored noise should spread the difference of power roughly equally over all the subcarriers. This remark will be verified numerically through simulations. Furthermore, very similar developments can be applied to INI from WS to NS. Therefore, the very same conclusion can be drawn for INI from WS to NS in OCDM-based multi-numerology systems.

V. Simulations Results

Simulations results aim at showing the performance of OCDM applied to multi-numerology system compared with OFDM signal, according to different metrics including: the per-subcarrier signal to INI ratio (SIR), the error vector magnitude (EVM), and the BER. All the figures have been obtained using matlab, considering an OCDM multi-numerology signal with two subcarrier spacing $\Delta_f^{NS} = 15$ kHz, $\Delta_f^{WS} = 30$ kHz, namely $R = 2$. Moreover, the CP length has been set to $N_{CP} = \frac{1}{16}N$ and $M_{CP} = \frac{1}{16}M$, a quadrature phase shift keying (QPSK) or a 16-quadrature amplitude modulation (QAM) constellation is considered, and both numerology signals share the same constellation size. All the results have been averaged over at least 10^4 simulations runs.

A first series of simulations shows the power spectrum of the OCDM composite signals x^{CP} (13) without filtering and $x^{CP,f}$ (19) with filtering versus the normalized frequency in Fig. 4 . They have been obtained using $K_N = 2K_W = 256$, and $L_f^{NS} = L_f^{WS} = 513$. A guard-band of $\Delta_f = 450$ kHz between NS and WS signals corresponds to 10 subcarriers of each signal. It can be observed that the side lobes power is reduced by about 120 dB in presence of the filter compared to the case without filter, and the guard-band emission is reduced as well. Thus, the addition of the filter can actually reduce the out-of-band emission such as expected, which is relevant in a context of spectrum scarcity or cognitive radio for instance. Besides, it should allow for a reduced INI, such as illustrated afterward. It must be noted that the very same spectrum can be obtained by considering OFDM instead of OCDM, but this is not shown in order not to overburden the figure.

Fig. 5 shows the SIR (dB) versus the subcarrier index (w.r.t. to NS) for non filtered and filtered OCDM composite signal and compared with OFDM. We recall that the SIR corresponds to the ratio between $\mathbb{E}\{|C_k|^2\}$ and $\mathbb{E}\{|\chi_k|^2\}$. The configuration is the same as previously, except that we set $\Delta_f = 0$ Hz, and we use a QPSK constellation. The term NS (resp. WS) in the legend refers to the considered subcarriers: NS (resp. WS) indicates that WS (resp. NS) signal interferes over NS (resp. WS) subcarriers. In order to fairly compare the INI over both NS and WS signals, we set $\gamma = \frac{M}{N}$.

It should be first noticed in Fig. 5 that the results regarding the OFDM composite signal are very similar to those obtained in [4], [5], which validates the simulations setup. Thus, the SIR degrades for edge subcarriers, *i.e.* those that are close to the other numerology (down to 0 dB for the non-filtered NS-OFDM), and the SIR at the WS subcarriers side is higher than NS subcarriers side. Furthermore, the filtering stage allows

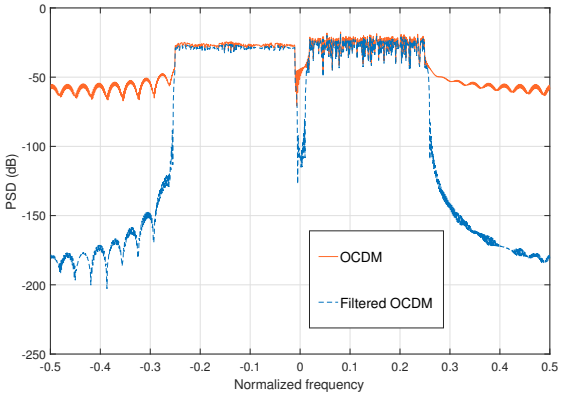

FIGURE 4. Power spectrum of multi-numerology OCDM signal with $\Delta f^{NS} = 15$ kHz, $\Delta f^{WS} = 30$ kHz, $\Delta f = 450$ kHz, and $L_f^{NS} = L_f^{WS} = 513$.

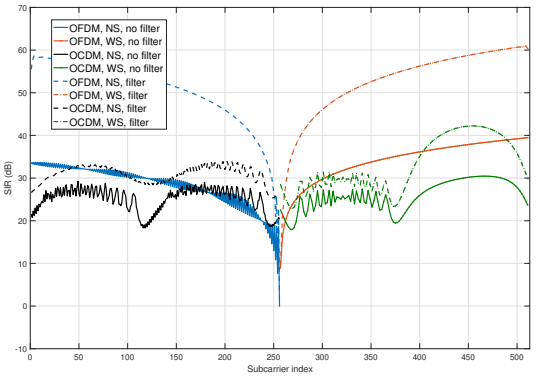

FIGURE 5. SIR (dB) versus subcarrier index (w.r.t to NS) for non filtered and filtered OCDM and OFDM. NS (resp. WS) indicates that WS (resp. NS) signal interferes over NS (resp. WS) subcarriers.

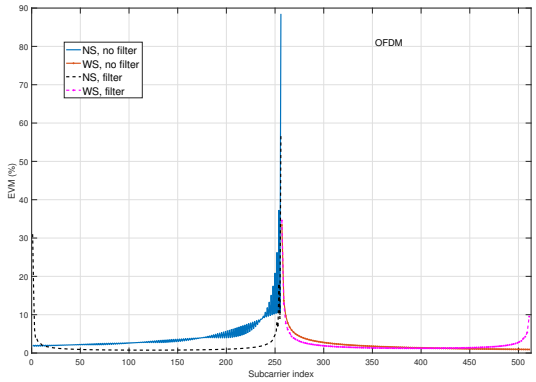

(a) OFDM.

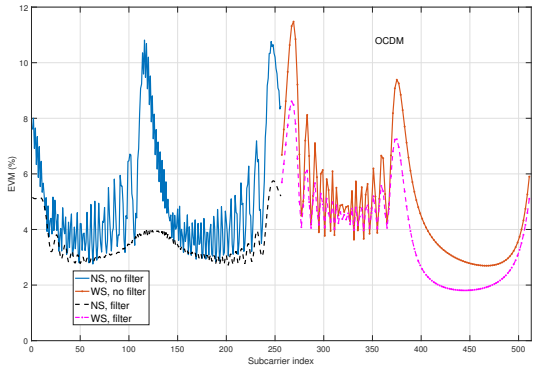

(b) OCDM.

FIGURE 6. EVM (%) versus subcarrier index (w.r.t to NS) for non filtered and filtered OFDM (a) and OCDM (b).

to largely increase the SIR except in this central area where it remains lower than 20 dB. In contrast, the SIR of the OCDM composite signal is more equally distributed over all subcarriers: the SIR for the non-filtered OCDM (NS as well as WS) slightly fluctuates between 18 and 28 dB, even in the area where the subcarriers of one numerology are close to the other numerology. This result confirms the analysis suggested below (34). In addition, this result also holds when filtering is added to the multi-numerology system. In that case, the SIR performance is improved by 5 to 10 dB over the whole subcarrier indices range.

Although results presented in Fig. 5 are interesting as it highlights the degradation due to the INI on subcarriers, the SIR does not take into account all the distortions affecting the signals, nor the overall system performance. For this reason, Fig. 6 shows the EVM (in %) versus subcarrier index (w.r.t to NS) for non filtered and filtered OFDM in Fig. 6-(a) and OCDM in Fig. 6-(b). The same simulation parameters as previously are considered. It should be first noticed that the EVM spans from 2% to 89% in OFDM-NS (from 2% to 35% in OFDM-WS) whereas it only spans from 2% to 11% in OCDM (irrespective of NS or WS). It confirms that the INI is spread over all subcarriers in OCDM, whereas it mainly concentrates near the center subcarriers in OFDM. Moreover, the filtered OFDM and OCDM signals outperform the non-filtered signals in general. However, we can observe in Fig. 6-(a) (OFDM) that the filtering also increases the EVM on the edges of the spectrum, mainly due to a phase rotation induced by the filter, which is not highlighted in the SIR in Fig. 5 since SIR is independent of the phase. In contrast, this additional distortion is concealed in OCDM since once again, it is spread over all subcarriers, therefore limiting EVM to low value ($< 12\%$).

To evaluate the overall system performance, Fig. 7 shows the BER versus the SNR (from -4 to 18 dB) of non filtered and filtered OCDM and OFDM, keeping the same parameters as previously, except that C_k are taken from a 16-QAM constellation. Note that we consider the overall BER including both NS and WS signals. Moreover, we also plot the case "No INI" as the lowest achievable bound of BER performance, which has been obtained by considering only one numerology (in the present case NS). We can observe on Fig. 7 that OCDM largely outperforms OFDM as OFDM reaches a lower bound of about BER=0.001 whereas OCDM

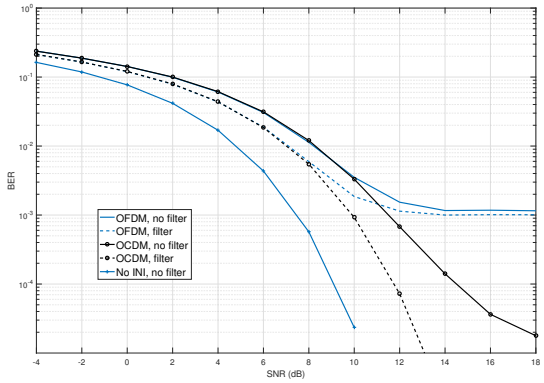

FIGURE 7. BER versus SNR (dB) for non filtered and filtered OCDM and OFDM.

does not in the considered SNR range. This is due, once again, to the inherent capability of OCDM to spread the errors due to INI (and filtering) equally over all subcarriers. In addition, we observe that filtered OFDM achieves better performance than non-filtered OFDM mainly in low SNR range, due to the effect of low-pass filter that reduces the noise besides the INI. However, filtered OFDM reaches the same lower bound as non-filtered OFDM, mainly due to the distortions induced by the filter, such as observed in Fig. 6-(a). In contrast, filtered OCDM outperforms non-filtered OCDM for any SNR value, and achieves only a 2dB loss compared with the case "No INI". To improve the performance of OFDM-based multi-numerology system, it should be then mandatory to apply a guard-band between NS and WS, to the cost of a loss of spectral efficiency. Unlike OFDM, (filtered)-OCDM is robust against the INI and the distortion due to the filtering without the need for a guard-band, and is then a good candidate for multi-numerology communication scheme, and in particular in case of spectrum scarcity such as shown in Fig. 4.

VI. Conclusion

In this paper, we have introduced a multi-numerology system based on the OCDM modulation scheme for possible application to future 6G communications. The OCDM signal has first been presented, and we detailed how it can be adapted to multi-numerology. In addition, the filtered-OCDM signal can also be used in such a flexible system, allowing for a reduction of both INI and out-of-band emission, therefore making the overall system compliant with spectrum scarcity use cases while keeping flexibility of multi-numerology. Then, the expression of the INI is analytically derived from the expression of the received signal with interference. Simulations results confirm the observation that the INI is spread over all subcarriers roughly equally in OCDM, while it is concentrated on the edge subcarriers in OFDM. It results that the BER performance of the (filtered-)OCDM is greatly better than that of the (filtered-)OFDM without need for a guard-band. We then conclude that OCDM is also a promising waveform that proves its relevance in the context of flexible multi-numerology systems. The future works should include the adaptation of some OFDM-based techniques to OCDM to further reduce the INI and improve the performance. Otherwise, it would be interesting to analyze in what extent it would possible to adapt other waveforms such as OTFS or AFDM to multi-numerology systems.

APPENDIX A
Proof of (2)

The case where N is even has been investigated in [20], and is hereby detailed. Thus, for any $m \in \{0, 1, .., N-1\}$ we have:

$$\begin{aligned} X_m =& \frac{1}{N}\sum_{n=0}^{N-1} x_n e^{-2j\pi\frac{mn}{N}} \\ =& \frac{e^{j\frac{\pi}{4}}}{N^2}\sum_{n=0}^{N-1}\sum_{k=0}^{N-1} C_k e^{-j\frac{\pi}{N}(n-k)^2} e^{-2j\pi\frac{mn}{N}} \\ =& \frac{e^{j\frac{\pi}{4}}}{N^2}\sum_{k=0}^{N-1} C_k e^{-j\frac{\pi}{N}k^2}\sum_{n=0}^{N-1} e^{j\frac{\pi}{N}(-n^2+2n(k-m))}, \end{aligned} \tag{35}$$

where we can recognize a generalized Gauss sum in the second sum indexed with n. Then, by noticing that $N \neq 0$ and $-N + 2(k-m)$ is even, we can apply Theorem 1.2.2 in [22] to obtain:

$$\begin{aligned} \sum_{n=0}^{N-1} e^{j\frac{\pi}{N}(-n^2+2n(k-m))} =& \sqrt{N} e^{j\pi\frac{N-4(k-m)^2}{-4N}} \sum_{n=0}^{0} e^{j\pi(Nn^2+2(k-m)n)} \\ =& \sqrt{N} e^{-j\frac{\pi}{4}} e^{j\frac{\pi}{N}(k-m)^2}. \end{aligned} \tag{36}$$

Finally, substituting (36) into (35) leads to:

$$X_m = \frac{\sqrt{N}}{N^2}\sum_{k=0}^{N-1} C_k e^{j\frac{\pi}{N}(m^2-2km)}, \tag{37}$$

such as given in (2).

In the case where N is odd, X_m can be developed as:

$$\begin{aligned} X_m =& \frac{e^{j\frac{\pi}{4}}}{N^2}\sum_{n=0}^{N-1}\sum_{k=0}^{N-1} C_k e^{-j\frac{\pi}{N}(n-k+\frac{1}{2})^2} e^{-2j\pi\frac{mn}{N}} \\ =& \frac{e^{j\frac{\pi}{4}-j\frac{\pi}{4N}}}{N^2}\sum_{k=0}^{N-1} C_k e^{-j\frac{\pi}{N}(k^2-k)}\sum_{n=0}^{N-1} e^{j\frac{\pi}{N}(-n^2+n(2(k-m)-1))}. \end{aligned} \tag{38}$$

Once again, we can use Theorem 1.2.2 in [22] by noticing that $N \neq 0$ and $-N + 2(k-m) - 1$ is even (since N is odd), leading to:

$$\sum_{n=0}^{N-1} e^{j\frac{\pi}{N}(-n^2+n(2(k-m)+1))} = \sqrt{N} e^{-j\pi\frac{N-(2(k-m)-1)^2}{4N}}. \tag{39}$$

Then, by substituting (39) into (38), we obtain

$$X_m = \frac{\sqrt{N}e^{j\frac{\pi}{4}-j\frac{\pi}{4N}}}{N^2}\sum_{k=0}^{N-1} C_k e^{-j\frac{\pi}{N}(k^2-k)} e^{-j\pi\frac{N-(2(k-m)-1)^2}{4N}} = \frac{\sqrt{N}}{N^2}\sum_{k=0}^{N-1} C_k e^{-j\frac{\pi}{N}(m^2+m(1-2k))}, \quad (40)$$

such as given in the case N odd in (2), which concludes the proof.

APPENDIX B
Proof of (26) and (27)

We first develop the expression of A in (25) by splitting the sum into R shorter sums:

$$A = \frac{1}{N}\sum_{n=0}^{N-1}\sum_{r=0}^{R-1} y_{n,r}^{WS,I} e^{-2j\pi\frac{pn}{N}} = \sum_{r=0}^{R-1} \underbrace{\frac{1}{N}\sum_{n=0}^{N-1} y_{n,r}^{WS,I} e^{-2j\pi\frac{pn}{N}}}_{\phi_{p,r}^{WS}}, \quad (41)$$

where $\phi_{p,r}^{WS}$ is defined for clarity purpose, and $y_{n,r}^{WS,I}$ is given in (21). Then, for $r = 0$, and by using the sum of terms of a geometric series, we obtain:

$$\begin{aligned}\phi_{p,0}^{WS} &= \frac{1}{N}\sum_{n=0}^{D_0-1} y_{n,0}^{WS,I} e^{-2j\pi\frac{pn}{N}} \\ &= \frac{1}{N}\sum_{n=0}^{D_0-1}\sum_{m=0}^{M-1} X_{m,0}^{WS} e^{2j\pi\frac{m}{M}(n+N_{CP}-M_{CP})} e^{-2j\pi\frac{pn}{N}} \\ &= \frac{1}{N}\sum_{m=0}^{M-1} X_{m,0}^{WS} e^{2j\pi\frac{m}{M}(N_{CP}-M_{CP})}\sum_{n=0}^{D_0-1} e^{2j\pi n(\frac{m}{M}-\frac{p}{N})} \\ &= \frac{1}{N}\sum_{m=0}^{M-1} X_{m,0}^{WS} e^{2j\pi\frac{m}{M}(N_{CP}-M_{CP})} \underbrace{\frac{1-e^{2j\pi D_0(\frac{m}{M}-\frac{p}{N})}}{1-e^{2j\pi(\frac{m}{M}-\frac{p}{N})}}}_{\text{asinc}_{D_0}(\frac{m}{M}-\frac{p}{N})}. \end{aligned} \quad (42)$$

For any other $1 \le r \le R-1$, the development is carried out by setting $n' = n - \Gamma_r$ where Γ_r is defined in (30), and by using the cyclic property of the CP to simplify $\phi_{p,r}^{WS}$ as follows:

$$\begin{aligned}\phi_{p,r}^{WS} &= \frac{1}{N}\sum_{n=r(M+M_{CP})-N_{CP}}^{(r+1)(M+M_{CP})-N_{CP}-1}\sum_{m=0}^{M-1} X_{m,r}^{WS} \\ &\quad \times e^{2j\pi\frac{m}{M}((n+N_{CP}-M_{CP}-r(M+M_{CP}))\mod M)} e^{-2j\pi\frac{pn}{N}} \\ &= \frac{1}{N}\sum_{n'=0}^{D_r-1}\sum_{m=0}^{M-1} X_{m,r}^{WS} e^{2j\pi\frac{m}{M}((n'-M_{CP}))\mod M)} e^{-2j\pi\frac{p}{N}(n'+\Gamma_r)} \\ &= \frac{e^{-2j\pi\frac{p\Gamma_r}{N}}}{N}\sum_{n'=0}^{D_r-1}\sum_{m=0}^{M-1} X_{m,r}^{WS} e^{2j\pi\frac{m}{M}(n'-M_{CP})} e^{-2j\pi\frac{pn'}{N}} \\ &= \frac{e^{-2j\pi\frac{p\Gamma_r}{N}}}{N}\sum_{m=0}^{M-1} X_{m,r}^{WS} e^{-2j\pi\frac{mM_{CP}}{M}}\sum_{n'=0}^{D_r-1} e^{2j\pi n'(\frac{m}{M}-\frac{p}{N})} \\ &= \frac{e^{-2j\pi\frac{p\Gamma_r}{N}}}{N}\sum_{m=0}^{M-1} X_{m,r}^{WS} e^{-2j\pi\frac{mM_{CP}}{M}} \underbrace{\frac{1-e^{2j\pi D_r(\frac{m}{M}-\frac{p}{N})}}{1-e^{2j\pi(\frac{m}{M}-\frac{p}{N})}}}_{\text{asinc}_{D_r}(\frac{m}{M}-\frac{p}{N})}. \end{aligned} \quad (43)\text{–}(44)$$

Then, for any $0 \le r \le R-1$, $0 \le k' \le K_N - 1$, and by setting $p' = p - Q_N$, we obtain $\chi_{k',r}^{WS}$ as follows:

$$\begin{aligned}\chi_{k',r}^{WS} &= \sum_{p=Q_N}^{Q_N+K_N-1} \phi_{p,r}^{WS} e^{-j\pi\frac{(p-Q_N)^2}{K_N}} e^{-2j\pi\frac{k'}{K_N}(p-Q_N)} \\ &= \sum_{p'=0}^{K_N-1} \phi_{p'+Q_N,r}^{WS} e^{-j\pi\frac{p'^2}{K_N}} e^{-2j\pi\frac{k'p'}{K_N}}, \end{aligned} \quad (45)$$

which leads to (27), and substituting A (41) with (42)-(44) into (25) and after straightforward rearrangements, we obtain (26), which concludes the proof.

APPENDIX C
Proof of (31)

Similarly to the developments carried out in Appendix B, we first express $\psi_{p,r}^{WS}$ for $Q_W \le p \le Q_W + K_W - 1$ and for any $r = 0, 1, .., R-1$ as the DFT of $y_{n,r}^{NS,I}$ in (24):

$$\begin{aligned}\psi_{p,r}^{WS} &= \frac{1}{M}\sum_{n=0}^{M-1} y_{n,r}^{NS,I} e^{-2j\pi\frac{np}{M}} \\ &= \frac{1}{M}\sum_{m=0}^{N-1} X_m e^{2j\pi\frac{m}{M}((r+1)M_{CP}-N_{CP})} \underbrace{\sum_{n=0}^{M-1} e^{2j\pi n(\frac{m}{N}-\frac{p}{M})}}_{\text{asinc}_M(\frac{m}{N}-\frac{p}{M})}. \end{aligned} \quad (46)$$

Then, by setting $p' = p - Q_W$, the multiplication by the conjugate chirp and the IDFT leads to:

$$\chi^{NS}_{k',r} = \sum_{p=Q_W}^{Q_W+K_W-1} \psi^{WS}_{p,r} e^{-j\pi\frac{(p-Q_W)^2}{K_W}} e^{2j\pi\frac{k'}{K_W}(p-Q_W)}$$
$$= \frac{1}{M} \sum_{p'=0}^{K_W-1} \sum_{m=0}^{N-1} X^{NS}_m e^{2j\pi\frac{m}{N}((r+1)M_{CP}-N_{CP})}$$
$$\times \text{asinc}_M\left(\frac{m}{N} - \frac{p'+Q_W}{M}\right) e^{-j\pi\frac{p'^2}{K_W}} e^{2j\pi\frac{k'p'}{K_W}}, \quad (47)$$

which concludes the proof.

REFERENCES

[1] X. Zhang, L. Chen, J. Qiu, and J. Abdoli, "On the Waveform for 5G," *IEEE Communications Magazine*, vol. 54, no. 11, pp. 74–80, November 2016.
[2] Z. E. Ankarali, B. Peköz, and H. Arslan, "Flexible Radio Access Beyond 5G: A Future Projection on Waveform, Numerology, and Frame Design Principles," *IEEE Access*, vol. 5, pp. 18 295–18 309, March 2017.
[3] 3GPP, "3GPP TS 38.211, Physical channels and modulation (Release 17, v17.3.0)," 3GPP, Tech. Rep., September 2022.
[4] X. Zhang, L. Zhang, P. Xiao, D. Ma, J. Wei, and Y. Xin, "Mixed Numerologies Interference Analysis and Inter-Numerology Interference Cancellation for Windowed OFDM Systems," *IEEE Transactions on Vehicular Technology*, vol. 67, no. 8, pp. 7047–7061, April 2018.
[5] A. B. Kihero, M. S. J. Solaija, A. Yazar, and H. Arslan, "Inter-Numerology Interference Analysis for 5G and Beyond," in *2018 IEEE Globecom Workshops (GC Wkshps)*, 2018, pp. 1–6.
[6] A. B. Kihero, M. S. J. Solaija, and H. Arslan, "Inter-Numerology Interference for Beyond 5G," *IEEE Access*, vol. 7, pp. 146 512–146 523, 2019.
[7] D. Demmer, R. Gerzaguet, J.-B. Doré, and D. Le Ruyet, "Analytical study of 5G NR eMBB co-existence," in *2018 25th International Conference on Telecommunications (ICT)*, June 2018, pp. 186–190.
[8] E. Memisoglu, A. B. Kihero, E. Basar, and H. Arslan, "Guard Band Reduction for 5G and Beyond Multiple Numerologies," *IEEE Communications Letters*, vol. 24, no. 3, pp. 644–647, December 2020.
[9] B. A. ÃĞevikgibi, A. M. DemirtaÅ§, T. Girici, and H. Arslan, "Inter-Numerology Interference Pre-Equalization for 5G Mixed-Numerology Communications," in *2022 IEEE 95th Vehicular Technology Conference: (VTC2022-Spring)*, June 2022, pp. 1–6.
[10] A. Yazar and H. Arslan, "Reliability enhancement in multi-numerology-based 5G new radio using INI-aware scheduling," *EURASIP Journal onWireless Communications and Networking*, vol. 2019, no. 110, pp. 1 – 14, December 2019.
[11] Q. Wang, A. Kakkavas, X. Gong, and R. A. Stirling-Gallacher, "Towards Integrated Sensing and Communications for 6G," in *2022 2nd IEEE International Symposium on Joint Communications & Sensing (JC&S)*, March 2022, pp. 1–6.
[12] R. Hadani, S. Rakib, M. Tsatsanis, A. Monk, A. J. Goldsmith, A. F. Molisch, and R. Calderbank, "Orthogonal time frequency space modulation," in *2017 IEEE Wireless Communications and Networking Conference (WCNC)*, 2017, pp. 1–6.
[13] X. Ouyang and J. Zhao, "Orthogonal chirp division multiplexing," *IEEE Transactions on Communications*, vol. 64, no. 9, pp. 3946–3957, 2016.
[14] T. Erseghe, N. Laurenti, and V. Cellini, "A multicarrier architecture based upon the affine Fourier transform," *IEEE Transactions on Communications*, vol. 53, no. 5, pp. 853–862, May 2005.
[15] A. Bemani, N. Ksairi, and M. Kountouris, "AFDM: A Full Diversity Next Generation Waveform for High Mobility Communications," in *2021 IEEE International Conference on Communications Workshops (ICC Workshops)*, June 2021, pp. 1–6.
[16] ——, "Affine Frequency Division Multiplexing for Next Generation Wireless Communications," *ArXiv*, pp. 1 – 30, May 2022.
[17] R. Bomfin, D. Zhang, M. MatthÄĪ, and G. Fettweis, "A Theoretical Framework for Optimizing Multicarrier Systems Under Time and/or Frequency-Selective Channels," *IEEE Communications Letters*, vol. 22, no. 11, pp. 2394–2397, 2018.
[18] R. Bomfin, M. Chafii, and G. Fettweis, "Low-Complexity Iterative Receiver for Orthogonal Chirp Division Multiplexing," in *2019 IEEE Wireless Communications and Networking Conference Workshop (WCNCW)*, 2019, pp. 1–6.
[19] M. S. Omar and X. Ma, "Spectrum design for orthogonal chirp division multiplexing transmissions," *IEEE Wireless Communications Letters*, vol. 9, no. 11, pp. 1990–1994, 2020.
[20] V. Savaux, "Flexible Communication System for 6G Based on Orthogonal Chirp Division Multiplexing," in *2022 1st International Conference on 6G Networking (6GNet)*, 2022, pp. 1–5.
[21] H. Huawei, "f-OFDM scheme and filter design, R1-165425," 3GPP, Tech. Rep., 2016.
[22] B. C. Berndt, R. J. Evans, and K. S. Williams, *Gauss and Jacobi Sums*. Ney York: John Wiley and Sons, 1996, ch. 1: Gauss Sums, pp. 7 – 56.

VINCENT SAVAUX received his engineering degree from the High School of Engineering, ECAM Rennes, an M.Sc. degree from the University of Rennes 1, France, in 2010, and his Ph.D. degree in telecommunications from Supélec in 2013. From 2014 to 2015, he was a post-doctoral researcher with the Signal, Communication, and Embedded Electronics (SCEE) Research Group, CentraleSupélec, Campus de Rennes, France. Since 2016, he has been a research engineer with the Advanced Connectivity Lab from the Institute of Research and Technology b<>com, Rennes, France. His research activities mainly focus on signal processing for wireless systems, including IoT technologies such as LoRa and NB-IoT, and digital communications for 5G and beyond 5G waveforms. He received the Exemplary Reviewer 2014 Appreciation from the IEEE WIRELESS COMMUNICATIONS LETTERS and the IEEE COMMUNICATIONS LETTERS.